PREPRINT UCRL-83312

CONF-791047--3

Lawrence Livermore Laboratory

RECENT PROGRESS IN INERTIAL CONFINEMENT FUSION AT THE LAWRENCE LIVERMORE LABORATORY

H. G. Ahlstrom and K. R. Manes

October 15, 1979

This paper was prepared for submission to the 11th Annual Electro Optics Conference, October 23-25, 1979
ANAHEIM, CA

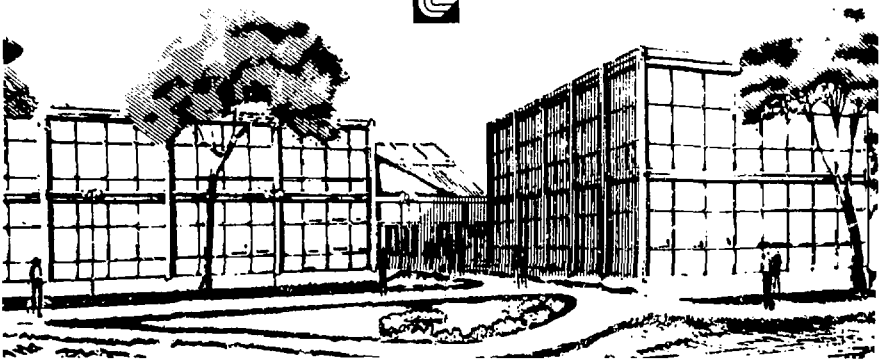

RECENT PROGRESS IN INERTIAL CONFINEMENT FUSION AT THE LAWRENCE LIVERMORE LABORATORY*

by

H. G. Ahlstrom and K. R. Manes
University of California, Lawrence Livermore Laboratory,
P. O. Box 5508, Livermore, California 94550

ABSTRACT

The Shiva and Argus laser systems at Livermore have been developed to study the physics of inertial confinement fusion. Both laser system designs are predicated on the use of large aperture Nd-glass disk amplifiers and high power spatial filters. During the past year we have irradiated DT filled microshell targets with and without polymer coatings. Recently new instruments have been developed to investigate implosion dynamics and to determine the maximum fuel density achieved by these imploded fusion pellets. A series of target irradiations with thin wall microshells at 15 to 20 TW, exploding pusher designs, resulted in a maximum neutron yield of 3×10^{10}. Polymer coated microshells designed for high compression were subjected to 4 kJ for 0.2 ns and reached fuel densities of 2.0 to 3.0 gm/cm^3. Results of these and other recent experiments will be reviewed.

*Work performed under the auspices of the U. S. Department of Energy by the Lawrence Livermore Laboratory under Contract No. W-7405-Eng-48.

I. INTRODUCTION

The basic concept of laser fusion has been described many times in the past.[1] Here we can summarize it in a simple statement of two requirements: fuel density times radius, $\rho r \geq 1$ gm/cm^2 and temperatures >5 keV. The intense focusing capability of the laser, 10^{14} to 10^{17} W/cm^2, is used to create a plasma at the surface of a spherical pellet. The heating of the plasma by the laser provides the energy required to ablate the surface of the pellet and compress the fuel to densities of a 1,000 to 10,000 x liquid density of DT. The implosion process is tailored so that at peak compression the fuel also achieves a temperature of approximately 5 keV. At these temperatures and densities and given $\rho r \geq 1$ g/cm^2 we will achieve efficient burn. As often pointed out, the reason for compressing the fuel is to achieve $\rho r \sim 1$ for pellet sizes which are sensible for fusion reactors. Since $r \sim C^{-2/3}$, where C is the compression, compressing the fuel to 1,000 x liquid density, reduces the requirement on the radius of the pellet by a factor of 100. Thus the goal of the Laser Fusion Program is to use lasers to demonstrate that these conditions can be achieved and thus prove the scientific feasibility of laser fusion.

Over the past several years, since 1974 at the Lawrence Livermore Laboratory, we have been pursuing these goals using a series of neodymium glass lasers as the driving sources. In Figure 1, we summarize our results and projections for the future in a chart where we plot the quality of inertial confinement, $n\tau$, which corresponds to ρr, versus the DT ion temperature. As seen in the figure, our experiments began with JANUS using a single beam in 1974 at a power of 0.2 TW. At that time we

were able to achieve an $n\tau$ of several times 10^{11} and approximately a 0.5 keV ion temperature. In 1975 with two beams from JANUS and 0.4 TW, we were able to increase the fuel temperature to approximately 2 keV with approximately the same value of $n\tau$. The major accomplishment in 1975 was the use of the α-particle spectrum to demonstrate that the fusion reactions produced were truly thermonuclear.[2] By 1976 we had developed ARGUS at 4 TW and had achieved ion temperatures of approximately 10 keV.

This whole series of experiments was done with a type of target which is called an exploding pusher.[3] The main idea in these experiments was to demonstrate that lasers could be used to meet the fusion temperature conditions albeit at low fuel densities. This lower path shows that SHIVA and NOVA, the next lasers coming on-line, could continue with this type of target and achieve higher values of $n\tau$. However, this type of target, with the energies available, will not attain break-even and is not a viable candidate for a fusion reactor target. In 1976 we also began our first series of experiments moving away from the exploding pusher concept in order to reach high densities although at relatively low fuel temperatures with current laser systems.[4] By 1978 with ARGUS at 2 kJ, we had achieved 10 x liquid density and early in 1979 with SHIVA at 8 kJ we had achieved a 100 x liquid density. The fuel temperature in these compressions is kept low, at approximately a half a kilovolt, to maximize the fuel compression and provide only a suffcient number of thermonuclear reactions for diagnostic purposes. The attainment of 100 x liquid density starting from significantly less than liquid density, is indeed a significant achievement. To reach this goal,

we had to provide for sufficiently uniform implosion of the target and, we had to achieve a condition which alleviated the problem of the Rayleigh-Taylor instability.[6]

The next step in the program, to achieve greater than 1,000 x liquid density, will also require significant developments. One is already in-hand, that is operation of SHIVA at its full energy potential of 15 kJ.[7] Target designs exist which project these fuel densities; however, they require innovations in the area of target fabrication. After once achieving 1,000 x liquid density, the program can then use this high density design to examine questions of stability through variations of the target parameters. We also plan to trade some of the final fuel density for temperature in order to produce a significant thermonuclear burn; e.g., by achieving temperatures of 2 keV at high densities. However, 2 keV, 50 x liquid density and projected fuel dimensions will not be sufficient for self-trapping of the 3.51 MeV α-particles within the fuel volume causing these α-particles to raise the temperature of the burning fuel. This boundary, called the ignition boundary, is not expected to be reached until we have at least the first phase of the NOVA system. This system is presently scheduled for completion in 1983 and the full NOVA system,[8],[9] which is expected to produce break-even or greater, will be ready in 1985.

II. EXPERIMENTAL ARRANGEMENTS

SHIVA, the system which we are now operating, is a twenty beam system with 2.5 cm and 5 cm diameter rod amplifiers; and 9 cm, 15 cm, and 20 cm diameter disk amplifiers. The system is assembled using the image relaying concept first put forward by John Hunt.[10] All twenty beams are fully diagnosed at the laser output to determine the energy, spatial distribution of energy, temporal profile of the output pulse, and any prepulses. The system utilizes twenty incident beam diagnostic packages, IBD, and twenty pointing focusing centering/reflected beam diagnostic packages, PFC/RBD.[11] The beams on SHIVA are arrayed in two clusters of ten which approximate the focusing cone of f/1 lenses. The beams are arranged so that each beam has an opposite member through a diagonal in the target chamber. Because each beam has its opposite member, the PFC/RBD system may be used for accurate alignment of the target at the focus of each one of the SHIVA beams as has been done on our two beam systems, JANUS and ARGUS. The upper and lower clusters consist of two pentagonal arrays of beams, an inner and an outer pentagon. The inner cluster is rotated 36° with respect to the outer cluster. This arrangement of the beams on SHIVA allows room in the equatorial region for target diagnostics. In Figure 2, we show an artist's view of the SHIVA target chamber with the beams arriving at the top and the bottom of the chamber and a number of the target diagnostic instruments that are used in the experiments.

An extremely important aspect of our program is to be able to measure the density in targets with relatively low ion temperature. One technique is by the activation of radio nuclides in the target material

to determine fuel and shell densities.[9],[12] The DT fusion reaction produces 14 MeV neutrons which then activate various materials in the target. If a seed material is placed in the fuel, it can be activated for direct determination of the fuel ρr. An average fuel density can then be calculated. The activation of other materials provides information about the density-radius product of those materials at the time of the burn of the fusion fuel.

More specifically, in Figure 3 we show schematically how the neutron from the fusion reaction could be used to determine the areal density of a SiO_2 pusher. Neutrons from the fusion reaction interacting with the ^{28}Si in the pusher produce ^{28}Al which is a radioactive nuclide. It has a beta-gamma decay with a half-life of 2.24 minutes. β's are emitted with an energy of 2.86 MeV and the γ's with an energy 1.78 MeV. As shown in the equation, if the neutron yield is measured independently, as in our experiments, and we are able to count the ^{28}Al atoms produced, we can determine the $\rho\Delta r$ of the pusher material. Knowing the $\rho\Delta r$ of the pusher material is of course very useful but we would like to also be able to relate that information to the fuel density. We can either relate the measured $\rho\Delta r$ of the pusher to the fuel density using our complex target simulation calculations or using a simple model. This simple fuel density-pusher areal density relationship assumes that the mass of the fuel and the glass pusher is conserved. We also make the assumption that the densities of the two materials are uniform although not equal. Finally, we make the observation that the pressure and temperature at the pusher-fuel interface must be continuous and equal and therefore, we will assume that the pressure and temperatures are uniform and equal throughout the pusher fuel regions.

Conservation of the masses of the fuel and pusher gives,

$$\frac{M_f(f)}{M_f(p)} = \frac{M_o(f)}{M_o(p)} \qquad \text{Eq. 1}$$

where the subscripts o and f represent the initial and final states respectively, and the f and p in brackets designate the fuel and pusher. Further, using the assumption of uniform densities in the fuel and the pusher, we can write,

$$\frac{\frac{4}{3}\pi\, r_f^{\,3}(f)\, \rho_f(f)}{\frac{4}{3}\pi \left[r_f^{\,3}(p) - r_f^{\,3}(f) \right] \rho_f(p)} = \frac{\frac{4}{3}\pi\, r_o^{\,3}(f)\, \rho_o(f)}{4\pi\, r_o^{\,2}(p)\, \rho_o(p)\, \Delta r_o} \qquad \text{Eq. 2}$$

where we have also assumed that the initial pusher thickness $\Delta r_o \ll r_o(f)$. Simple algebraic manipulation leads to,

$$\rho_f(f) = \rho_o(f) \left\{ \frac{\rho_f(p)}{\rho_o(p)} \frac{\Delta r_f}{\Delta r_o} \left[1 + \frac{2}{3} \frac{\Delta r_f}{r_f(f)} + \frac{1}{3} \left(\frac{\Delta r_f}{r_f(f)} \right)^2 \right] \right\}^{3/2} \qquad \text{Eq. 3}$$

For cases where $\Delta r_f / r_f(f) \ll 1$, we need no further assumptions. However, this is not generally true and we make the isobaric, isothermal assumption to obtain a relationship between $\rho_f(f)$ and $\rho_f(p)$. This leads to,

$$\rho(p) = a\, \rho(f) \qquad \text{Eq. 4}$$

where α is determined by the degree of ionization of the pusher material. We can then write,

$$\rho_f(f) = \left[\rho_f(p)\ \Delta r_f\right]^{3/2}\ G\left[M(p),\ M(f),\ \alpha\right] \qquad \text{Eq. 5}$$

Where

$$G = \left\{\alpha\left(\frac{3}{4\pi}\right)^{1/3}\left[\left(\frac{M(p)}{\alpha} + M(f)\right)^{1/3} - M(f)^{1/3}\right]\right\}^{-3/2}$$

Now let us examine for a moment how an experiment might be performed. In the analysis of the data one must know the fraction of the target collected in any collection system. It is well known in laser interaction experiments that a simple collector does not collect the geometrical fraction of target material that it intercepts. As a result, we must have a measure of the target fraction which is collected. One approach to solving this problem is to irradiate the target in a nuclear reactor with thermal neutrons to produce a radioactive tracer. For targets containing glass pushers, the ^{23}Na in the glass can be activated to produce ^{24}Na. ^{24}Na has a half-life of 15 hours and so the target may be counted before the experiment is performed. After the implosion, the ^{28}Al acitivity can be counted for 5 minutes and then the remaining ^{24}Na activity can be counted for 24 hours. A second counting of the ^{24}Na measures the target fraction collected allowing the determination the of ^{28}Al activity produced in the SiO_2 pusher.

In Figure 4 we show schematically how this system is implemented on SHIVA and we also show a multiple shell target which has been irradiated. The multiple shells, of course, each contain a material which could be activated by the neutrons from the fusion reaction thus providing information about the areal density of each one of the shells at the time of the fusion burn. In this system, the collector is an Al cylinder lined with reactor grade Ti or Ta foils. It is important that the collector foils not contain any trace materials which could be activated by the fusion neutrons and produce decay products which would confuse our counters. After the experiment has been performed, the aluminum cylinder is retracted automatically through a gate valve and then released through another valve to fall down through a plastic tube to the basement of the SHIVA system where the counting system is located.

The counting system consists of a 25.4 cm NaI crystal for measuring the gamma reactivity coupled with β and background counters.[13] It is a NaI well detector containing a NE 102 fluor system into which are inserted the Ti or Ta foils on which the activated material from the target has been deposited. The NE 102 β counting fluor consist of a cylinder around which the foils are wrapped and then cylinder and foils are placed inside another cylinder of NE 102 fluor. This combination is next placed inside the NaI fluor thus producing a system which has a 100% efficiency for counting the β decay and 40% efficiency for counting the γ ray decay, for a combined efficiency of 40%. Because of the extreme sensitivity of the large detector system to outside radiations, we place the counting station in the basement of SHIVA to provide concrete shielding against cosmic rays and other naturally, or artificially, occurring radioactivity. We also place the system inside a 10 cm thick lead chamber.

However, even with all of these precautions, we receive significant background due to cosmic rays which enter the NaI crystal, Compton scatter and produce coincidence counts in the NaI and NE 102 fluor systems. To reduce the background due to cosmic rays, we have surrounded the counting crystals with Geiger tubes to sense the arrival of cosmic rays which produce a triple coincidence in the counting system and are thus rejected. The background of this system in a five minute counting interval is two counts. The utilization of this system has produced an extremely low threshold for determining the $\rho\Delta r$ of glass pushers.

Another technique that we have developed to determine the size of the compressed fuel region is a spatially resolving crystal spectrometer designed to look at the line emission from argon contained in the fuel.[14] A crystal spectrometer is used to provide spectral discrimination and a slit perpendicular to the direction of the spectral dispersion provides spatial discrimination in one dimension. The limitation to this type of system is that as the pusher becomes more dense, the opacity for the propagation of the seed material line radiation through the pusher increases, eventually eliminating the possibility of transporting this radiation out to the detector. Therefore, as we go to pusher materials of higher density or higher opacity, we must employ seed materials with higher energy characteristic radiation. Increased fuel temperature will be required to generate this characteristic radiation.

In Figure 5 we summarize the density measuring capability of a number of different techniques. We plot the density confinement radius product as a function of the DT neutron yield. The various boundaries in the

figure represent the boundary of applicability of various density measuring techniques. In the past with low density targets, we have utilized imaging of the alpha particles to determine the size, shape, and distribution of the burning region.[15] In this figure, we clearly see that this technique is limited to exploding pusher targets since the upper boundary of the density confinement radius product is 10^{-3} g/cm^2. Hence this technique has no applicability for high density, intermediate yield targets. Of course, the technique can be used again when yields become high enough for imaging of the neutrons rather than the alpha particles.[9]

The four shaded regions labeled Ar, Br, Si, and Cu represent the useful operating regime of radiochemistry either of materials in the fuel, such as Ar or Br, or materials in the pusher, such as Si or Cu. Cu appears to offer a very significant advantage in that density radius products as high as 10^{-2} g/cm^2 can be measured with neutron yields as low as several times 10^4. The region of usefulness for the Si in the pusher is in the range of 10^6 to 10^8 neutrons. There is only a small shift over to the right for Br in the fuel and thus Br as a seed material in the fuel would be extremely useful in diagnosing the density of 100 x liquid density targets. Ar requires much higher yields, on the order of 10^{10}, to be useful for determining fuel density. The other boundary placed in this parameter space is the use of Ar imaging and here we show that as the neutron yield increases, the temperature of the fuel and pusher material are increasing thus reducing their opacity and making it possible to propagate the x-ray lines through the material surrounding

the fuel. In summary, it appears that Cu is an extremely useful material in the pusher in terms of activation for density determination. The material in the fuel that would be most useful is Br; however, Si is a readily available material which can provide information about fuel density for targets with glass pushers with $\rho\Delta r \simeq 10^{-2}$ g/cm^2.

SECTION III IMPLOSION EXPERIMENTS

The experiments that were performed on SHIVA as it was being brought into activation were all of the exploding pusher, low density nature. These experiments were designed to prove the quality of the laser operation. Consequently these studies were performed with single beam illumination, four beam illumination, ten beam illumination from one side, and finally with all twenty beams from both sides. After the system activation was complete, we began a series of experiments with all twenty beams to further demonstrate the performance of the system using the exploding pusher, low density targets.

The experiments and the calculations showed that most of the absorption occurred on the pole caps of the spherical microshell targets and that there was significant distortion from spherical symmetry in the implosion and burn of the fuel. This was further demonstrated by data taken with the alpha zone plate camera which images the distribution of the alpha particles from the burn. These data along with $\rho\Delta r$ measurement from the neutron activation of the SiO_2 pusher are shown in Figure 6. From the alpha zone plate data one would infer an average denisty of 0.1 g/cm^3 or approximately 0.5 x liquid density. The radiochemsitry measurement of the silicon pusher $\rho\Delta r$ gave a value of approximately 7×10^{-4} gm/cm^2. Using the simple theory of exploding pusher

targets[16] and more sophisticated simulation codes one can calculate the target performance which gives the fuel density and the $\rho\Delta r$ of the pusher. This calculation has been made and is in reasonable agreement with the alpha zone plate image data.

We have also used the argon line imaging technique with these exploding pusher targets since $\rho\Delta r < 10^{-3}$ gm/cm^2. A slitted spectrograph provided one dimensional spatial imaging of the emission from the fuel and corona regions. Potassium lines from the potassium trace element in the glass pusher produced images which extended out into the corona and also provided an image of the outer region of the stagnated pusher. The argon inside the glass microshell provided a spatial distribution of the helium-like and the hydrogen-like alpha lines. These lines were well resolved spectrally and produced distributions which had base widths of approximately 50 μm and 45 μm respectively. The difference in the spatial extent of the helium-like and hydrogen-like lines implies either a temperature gradient across the fuel pusher interface or, more likely, the time integration effect due to the temperature rising as the stagnation of the pusher and the fuel occurs. As the pusher and fuel stagnate, the temperature rises rapidly and one would expect that the helium-like lines would be excited before the hydrogen-like lines, and, therefore, the spatial extent of the helium-like lines would be expected to be greater than that of the hydrogen-like lines. The point to be made here is that any time integrated emission from the fuel region requires significant code interpretation to determine the density and is not a simple straightforward diagnostic of the final fuel density.

We have also implemented our zone plate camera in the coded imaging mode to image the high energy x-rays from the fuel region. Figure 7 shows one of our gold zone plates which has been fitted with a stack of films and filters designed to guarantee a large dynamic range for an individual energy and to produce images at successively higher energies through the film stack. This technique overlaps with our Kirkpatrick-Baez and Wolter x-ray microscopes and extends our coverage to higher energies.

IV SUMMARY

In Figure 8 we summarize the density and neutron yield achieved for three classes of targets. The data in the lower right hand corner at neutron yields of the order of 10^{10} are from exploding pusher targets irradiated with SHIVA. The density in this case is determined by alpha imaging and typically we reach approximately 0.5 - 1.0 x liquid density starting from densities of about .01 x liquid density. The second class of targets typically achieved from 4 - 10 x liquid density. As can be seen, we produced lower neutron yield in these experiments while we compressed the fuel to essentially a factor of ten higher density. The last series of experiments achieved densities in the range of 40 to 150 x liquid density and again we were forced to lower the final fuel temperature in order to reach these densities.

In the coming years, as we continue to push to higher densities, the things that must be done are to operate SHIVA at its full energy capability for nanosecond and longer pulses and to fabricate the targets which have been designed to achieve these higher densities. The success of the program in carrying out ablative driven implosion experiments over

the last year, gives us a high degree of confidence in meeting the fabrication requirements, the laser irradiation requirements and realizing the diagnostics needed to measure the achieved densities. The program is now well on its way towards densities of interest for inertial confinement fusion reactors. In fact, the $n\tau$ products are now in the range of several times 10^{14}. We have already demonstrated, with low density implosion targets, that we can achieve the temperatures required for ignition. So now the problem remains to achieve densities in the range of 1,000 to 10,000 x liquid density and at the same time drive the target to temperatures appropriate to ignition, break even and finally net energy gain.

Acknowledgments

The work reported here represents but a portion of the combined efforts of the workers in three major program elements at the Lawrence Livermore Laboratory during the past year. Results mentioned originate from H. Ahlstrom's Fusion Experiments Program, J. Holzrichter's Solid State Laser Program and J. Nuckolls' Target Design and Fabrication Program.

REFERENCES

1. J. Nuckolls, L. Wood, A. Thiessen, G. Zimmerman, Nature 239, 139, 1972.

2. V. W. Slivinsky, H. G. Ahlstrom, R. G. Tirsell, J. Larsen, S. Glaros, G. Zimmerman, and H. Shay, "Measurement of the Ion Temperature in Laser Driven Fusion," Phys. Rev. Letts., Vol. 35, No. 16, pp. 1083-1085, 20 October 1975.

3. Glen Dahlbacka and John Nuckolls, Laser Driven Isothermal Implosions, Lawrence Livermore Laboratory UCRL 75885, 28 October 1974.

4. J. M. Auerbach, et. al., "Neon Spectral Line Broadening as a Diagnostic for Compressed Laser Fusion Targets," J. of App. Phys., July 1979.

5. LLL Laser Fusion Monthly, MM 79 2, February 1979.

6. J. D. Lindl and W. C. Mead, "Two Dimensional Simulation of Fluid Instability in Laser Fusion Pellets," Phys. Rev. Letts., Vol. 34, No. 20, pp. 1273-1276, 19 May 1975.

7. D. R. Speck, et. al., "Performance of the Shiva Laser Fusion Facility," LLL UCRL 82117, presented at the 1979 IEEE/OSA Conference on Laser Engineering and Applications, Washington, D.C., May 30 - June 1, 1979.

8. T. J. Gilmartin, "Nova, the Laser Fusion Scientific Feasibility Experiment," LLL UCRL 82094, presented at the 1979 IEEE/OSA Conference on Laser Engineering and Applications, Washington, D.C. May 30 - June 1, 1979.

9. H. G. Ahlstrom, et. al., "Diagnostics of Shiva Nova High Yield Thermonuclear Events," J. Opt. Soc. Am., Vol. 68, No. 12, pp. 1731-1741, December 1978.

10. J. T. Hunt, et. al., "Improved Performance of Fusion Lasers using the Imaging Properties of Multiple Spatial Filters," Applied Optics Vol. 16, No. 4, pp. 779-782, April 1977.

11. E. S. Bliss, et. al., "Beam Alignment," LLL Laser Program Annual Report, UCRL 50021-76, pp. 2-141/2-145, 1976.

    F. W. Holloway, et. al., "Alignment Control Subsystem," LLL Laser Program Annual Report, UCRL 50021-76, pp. 2-147/2-155, 1976.

    R. G. Ozarski, et. al., "Beam Diagnostics," LLL Laser Program Annual Report, UCRL 50021-76, pp. 2-155/2-169, 1976.

    W. C. O'Neal, et. al., "Targent Chamber," LLL Laser Program Annual Report, UCRL 50021-76, pp. 2-169/2-181, 1976.

12. E. M. Campbell, "Diagnostics of High Density Targets by Neutron Activation Techniques," Bull. Am. Phys. Soc., Vol. 23, No. 7, pp. 803, September 1978.

E. M. Campbell, "Collection Fraction Determination Utilizing a Radioactive Tracer," being prepared for submission to J. of App. Phys.

E. M. Campbell, "Fuel ρR of ICF Targets by Neutron Activation," being prepared for submission to J. of App. Phys.

13. E. M. Campbell, "Exploding Pusher Tamper ρΔR Measurement by Neutron Activation," being prepared for submission to Phys. Rev. Letts.

14. L. N. Koppel, et. al., "Diagnosis of Laser Produced Implosions using Argon X-Ray Lines," being prepared for submission to Phys. Rev. Letts.

15. N. M. Ceglio and L. W. Coleman, "Spatially Resolved Emission from Laser Fusion Targets," Phys. Rev. Letts., Vol. 39, No. 1, pp. 20-24, 4 July 1977.

16. E. K. Storm, "A Simple Model for Exploding Pusher Targets," LLL Laser Program Annual Report, LLL UCRL 50021-77, pp. 6-38/6-46, 1977.

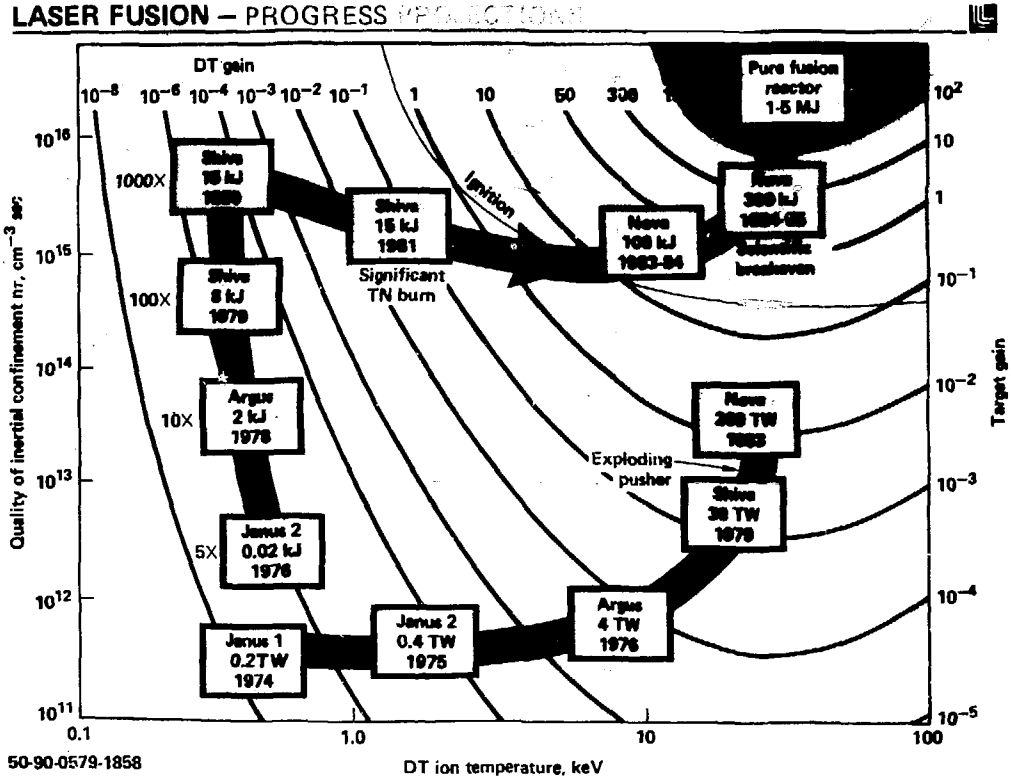
LASER FUSION – PROGRESS
DT gain
10^{-8} 10^{-6} 10^{-4} 10^{-3} 10^{-2} 10^{-1} 1 10 50
Pure fusion reactor 1-5 MJ
Ignition
Shiva 15 kJ 1981
Significant TN burn
Nova 100 kJ 1983-84
Nova 300 kJ 1984-85
Scientific breakeven
1000X
Shiva 10 kJ 1979
100X
Shiva 5 kJ 1979
Argus 2 kJ 1978
10X
Janus 2 0.02 kJ 1976
5X
Janus 1 0.2TW 1974
Janus 2 0.4 TW 1975
Argus 4 TW 1976
Nova 200 TW 1983
Exploding pusher
Shiva 30 TW 1979
10^{16}
10^{15}
10^{14}
10^{13}
10^{12}
10^{11}
Quality of inertial confinement nτ, cm^{-3} sec
10^{2}
10
1
10^{-1}
10^{-2}
10^{-3}
10^{-4}
10^{-5}
Target gain
0.1
1.0
10
100
DT ion temperature, keV
50-90-0579-1858

Figure 1

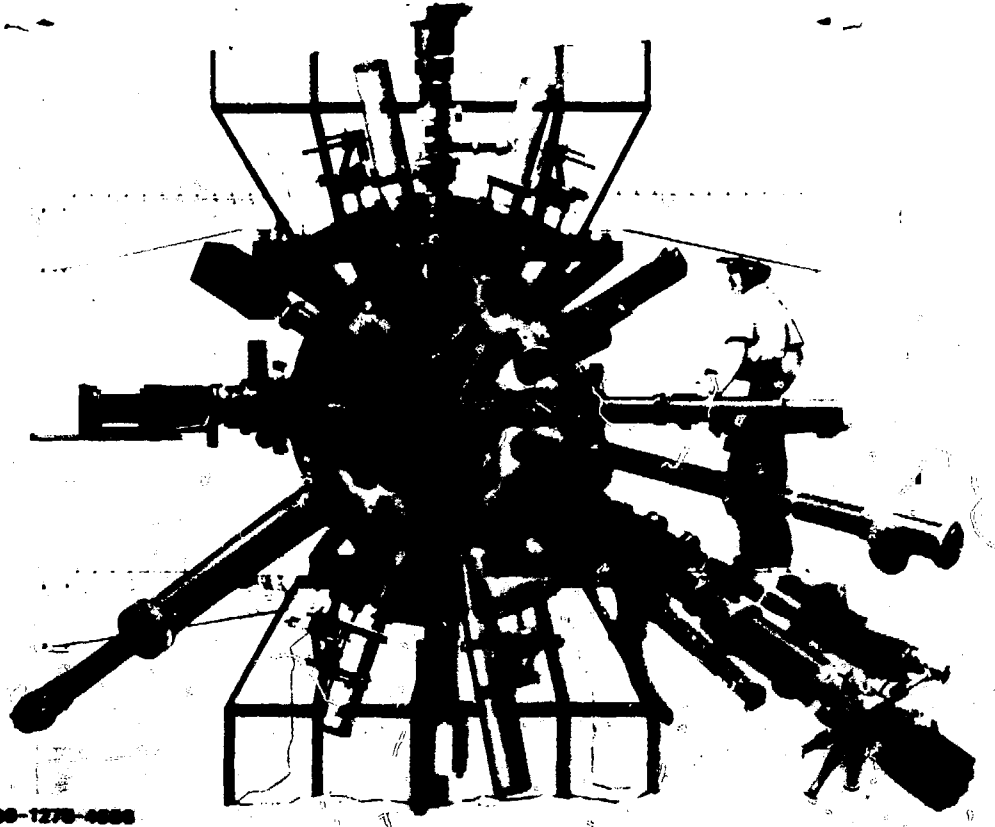

Figure 2

THE EFFECTIVE $\rho\Delta R$ OF THE GLASS MICROSPHERE IS DETERMINED BY MEANS OF "RADIOCHEMISTRY"

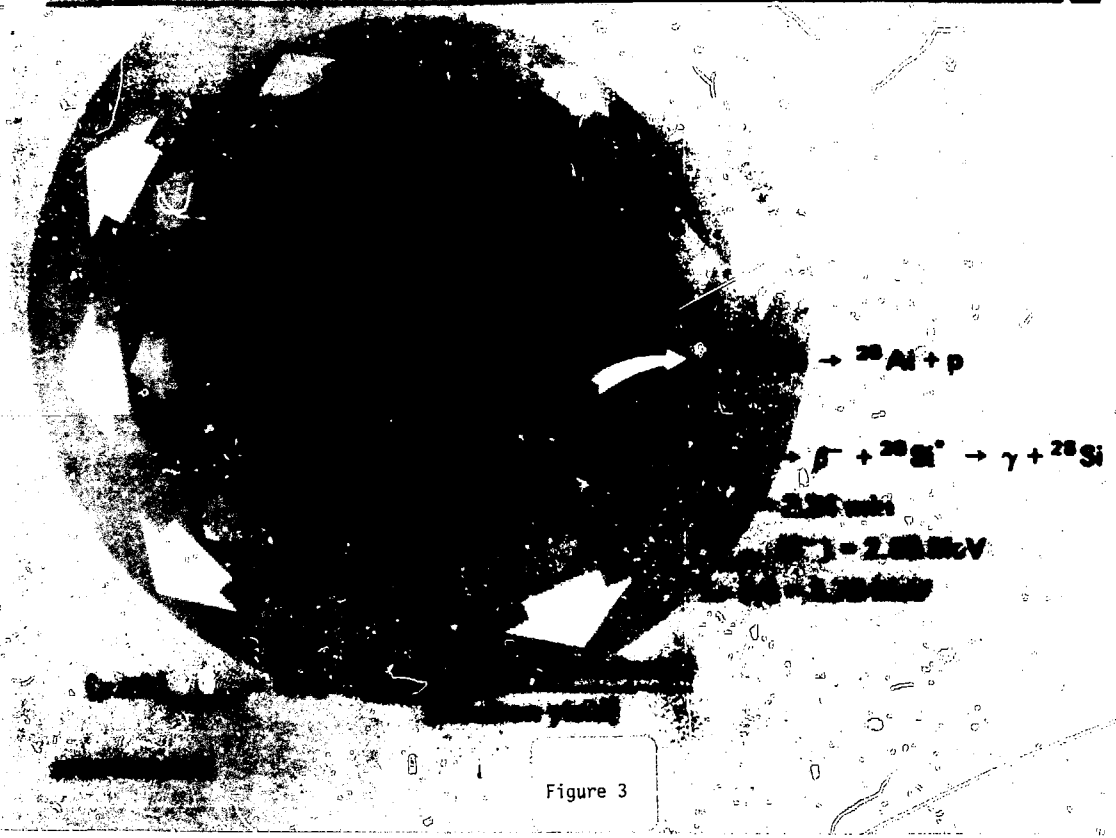

Figure 3

Density Measurements by Neutron Activation

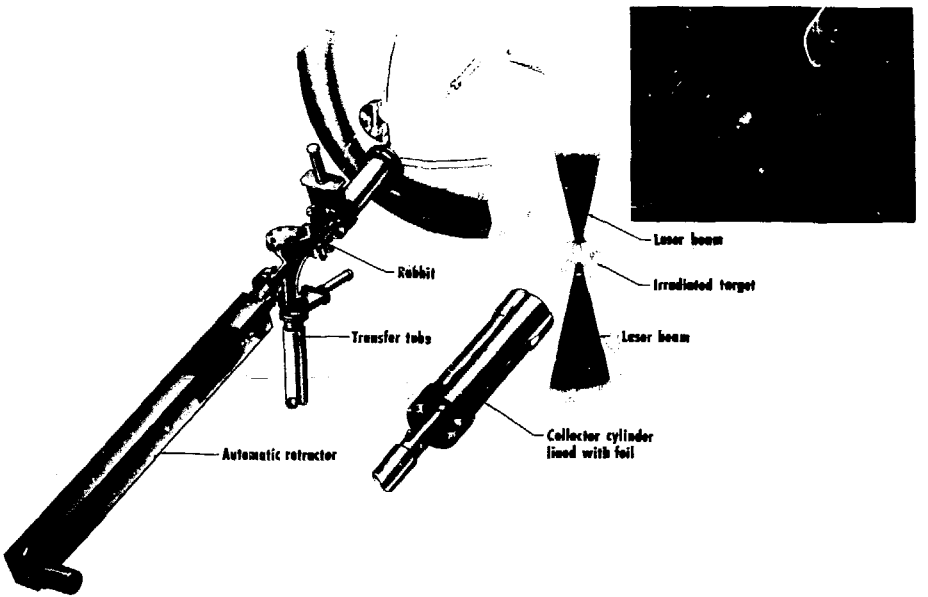

Figure 4

PRESENT DENSITY DIAGNOSTIC OPERATING REGIMES

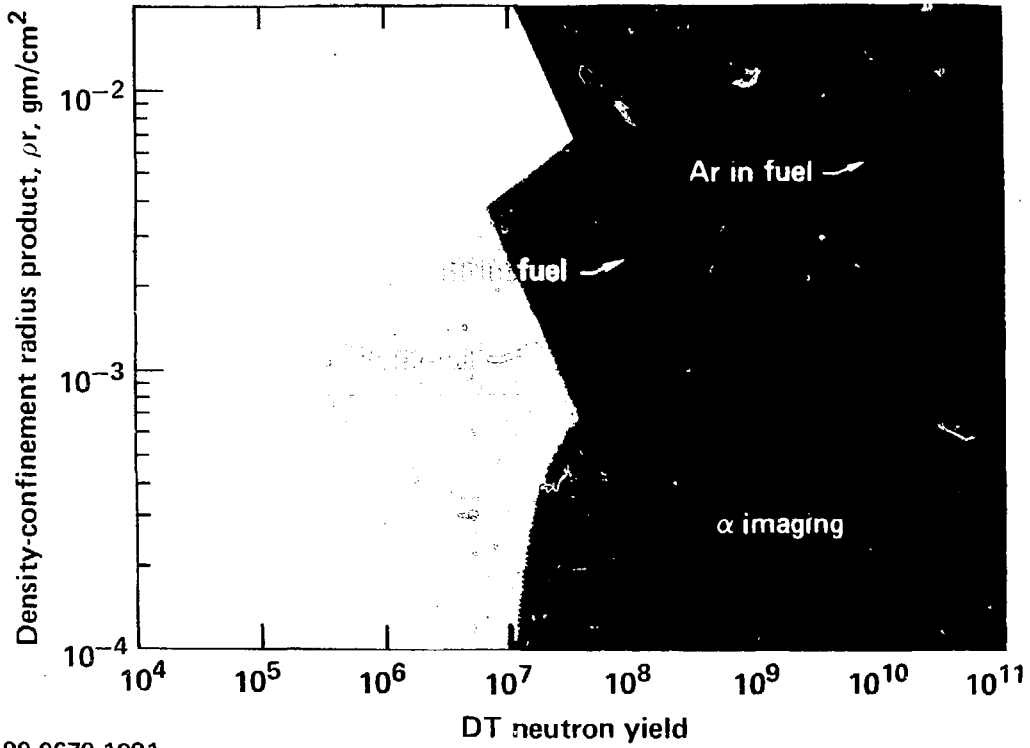

20-90-0679-1891

Figure 5

NEUTRON ACTIVATION

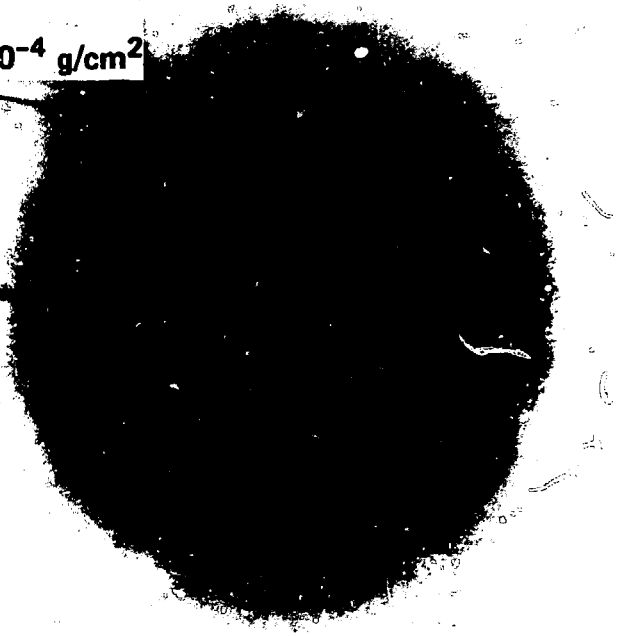

20-50-0579-1607

Figure 6

MULTI-SPECTRAL X-RAY IMAGING OF COMPRESSED HIGH DENSITY TARGET (TECHNIQUE)

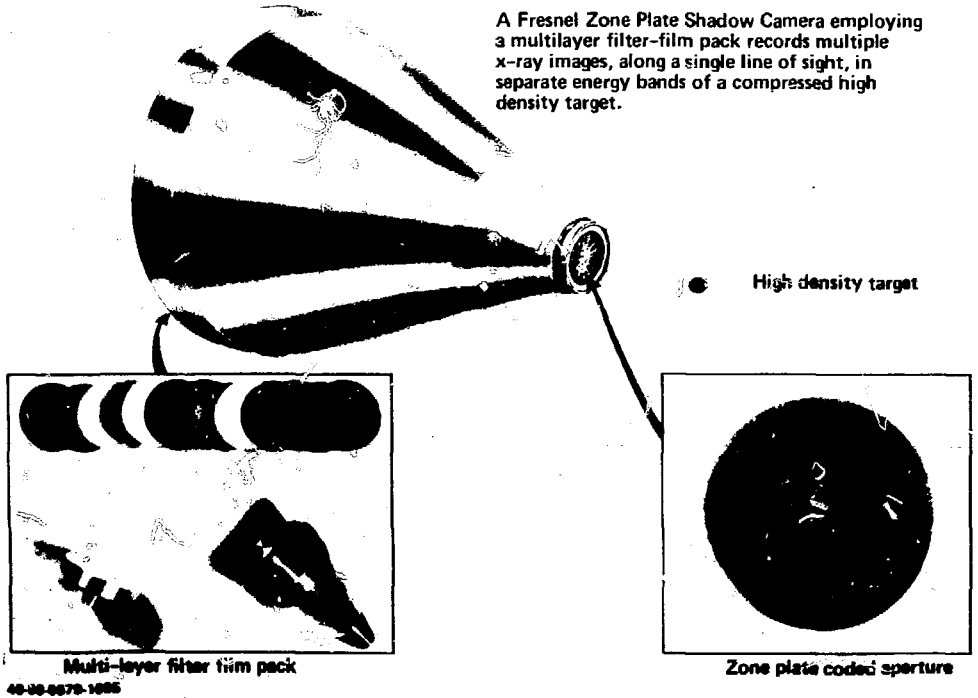

Figure 7

FUEL DENSITY AT BURN TIME VERSUS NEUTRON YIELD

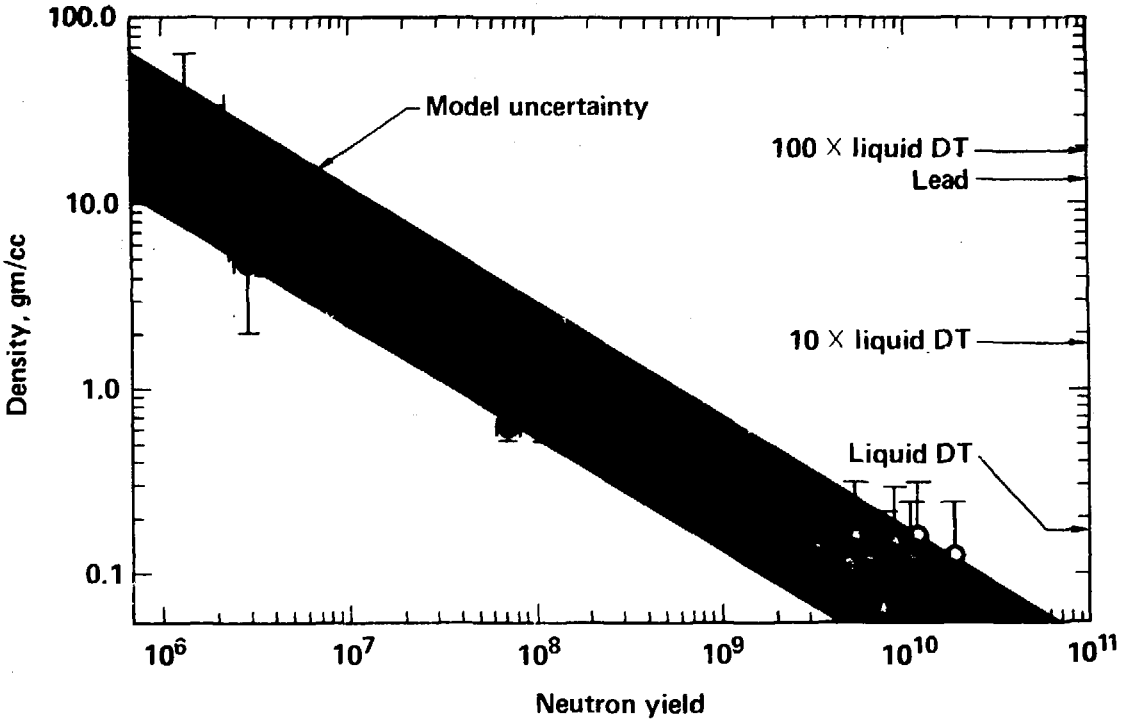

20-15-0579-1727

Figure 3